Field calibration techniques used to characterize the radiometric stability of the GEO-CAPE Airborne Simulator (GCAS)

Peter Pantina*[a,c], Matthew G. Kowalewski[b,c], Scott J. Janz[c], Sanxiong Xiong[a,c]
[a]Science Systems and Applications, Inc., Lanham, MD USA 20706;
[b]Universities Space Research Association, Columbia, MD USA 21046;
[c]NASA Goddard Space Flight Center, Greenbelt, MD USA 20771

ABSTRACT

The GEOstationary Coastal and Air Pollution Events (GEO-CAPE) Airborne Simulator (GCAS) was developed at NASA's Goddard Space Flight Center (GSFC) and has flown in multiple field campaigns to perform mapping of the regional-scale EPA criteria pollutants nitrogen dioxide, ozone, and formaldehyde. GCAS will also participate in validation campaigns for NASA's Tropospheric Emissions: Monitoring POllution (TEMPO) mission and the Korean Geostationary Environment Monitoring Spectrometer (GEMS) mission, both scheduled to launch in the early 2020s. GCAS houses two commercial Offner-type grating spectrometers that measure backscattered solar spectral radiance from the near-ultraviolet to near-infrared at high spatial resolution (typically 250 meters at 8.5 kilometer altitude). These radiances are used to retrieve spatial and temporal distributions of trace gases relevant to the boundary layer and free tropospheric atmospheric chemistry cycles.

In this paper, we describe the field calibration techniques employed to characterize the spectral and temporal radiometric stability of the system during its most recent deployment in the 2018 Long Island Sound Trace Ozone Study (LISTOS) field campaign. Overall measurement uncertainty, retrieval impacts, and lessons learned for future deployments will also be described.

Keywords: airborne, remote sensing, spectrometer, calibration, radiometry, trace gas

1 INTRODUCTION

1.1 GeoCAPE Airborne Simulator (GCAS)

GCAS was designed and built at the Radiometric Calibration and Development Laboratory (RCDF) at NASA Goddard Space Flight Center (GSFC) to demonstrate the potential of high precision, compact, and easily deployable spectrographs; to refine science measurement requirements for the GEO-CAPE atmospheric science study group; and to provide regional test case data for geostationary trace gas retrieval algorithm development. It is anticipated that the instrument will be a primary component in future validation campaigns for NASA's Tropospheric Emissions: Monitoring POllution (TEMPO) air quality monitor and the Korean Geostationary Environmental Monitoring Spectrometer (GEMS) missions, both scheduled to launch in the early 2020s. Since 2013, GCAS has flown on several NASA aircraft, and data collected from those platforms have been used to map regional-scale air pollution distribution and to identify point sources at several locations, both domestic and international.[7],[15],[4]

GCAS houses two commercial Offner-type grating spectrometers that simultaneously measure backscattered solar spectral radiance in the wavelength regions of 305 nm – 490 nm and 480 nm – 900 nm. We will refer to these spectrometers as the air quality (AQ) and ocean color (OC) spectrometers, respectively. Radiances from the AQ

(particularly from 300 nm – 350 nm) are calculated and then post-processed to retrieve spatial and temporal distributions of ozone, sulfur dioxide, nitrogen dioxide, formaldehyde, and other species relevant to atmospheric chemistry cycles. These retrievals typically use relative spectral radiances, and as such relative (band-to-band) calibration is most important in these cases. Although not the focus of this manuscript, radiances from the OC may be used to monitor ocean color and related properties, including phytoplankton concentrations. These measurements have implications for climate and ecological research [18] and the retrieval algorithms for the relevant productivity products require very accurate absolutely calibrated spectral radiances.[20]

1.2 Importance of atmospheric retrievals and calibrations

Both boundary layer ozone and nitrogen oxides have well-known effects on human health, leading to disease and premature death, particularly in industrializing countries where levels of air pollution are high.[1],[6] Past studies have also demonstrated that global tropospheric nitrogen dioxide and ozone concentrations have significantly increased over the past decades, altering radiative forcing in the process.[16] GCAS was designed to act as a satellite simulator over targeted urban areas to assist in the planning, algorithm development, and validation of future geostationary satellite instruments such as TEMPO and GEMS, which will focus on monitoring these species and understanding their lifecycles and long-term trends in abundance.

To ensure reliable retrievals with "lifetime stability"[11] and cross-comparability with upcoming satellite data, we require robust, repeatable instrument calibrations between campaigns and individual flights, defined by a set of standard operating procedures[17] and calibration standards. By monitoring the calibration results over time, particularly before and after each field deployment, we can better understand how short-term changes in spectral or spatial response may be affecting the observations. Consistent calibrations help to identify sensor problems, before they manifest themselves as data artifacts, and to develop better correction algorithms to post-process raw data.[19]

Several studies have shown the benefit of careful calibrations on subsequent atmospheric retrievals. For example, improvements in dark signal calibration routines resulted in significantly improved carbon dioxide and methane retrievals from the SCanning Imaging Absorption SpectroMeter for Atmospheric ChartographY (SCIAMACHY).[3] The Ozone Monitoring Instrument (OMI) retrievals of ozone, nitrogen dioxide and formaldehyde were similarly improved with dark signal calibration routine enhancements.[12] Those results were highly dependent on small, spectral absorption features that were sensitive to the spectral stability and spectral slit function of the instrument.

1.3 Field campaign

GCAS was based at the NASA Langley Research Center during the summer of 2018 to participate in the Long Island Sound Tropospheric Ozone Study (LISTOS) field campaign from 18 June – 6 September.[14] The study focused on understanding and quantifying ozone chemistry and transport from New York City to downwind areas, particularly across the waters of Long Island Sound and the Connecticut coast.

From 3 July – 6 September 2018, GCAS recorded data on science flights aboard a NASA Bombardier B-200 aircraft. Due to instrument swaps and aircraft maintenance, GCAS was removed and reinstalled at least three times during the evolution of the study. Although we expect no change in GCAS performance between integrations, systematic differences in installation position (affecting viewing geometric or ambient operating conditions) could potentially affect observed radiances and subsequent retrievals,[2] particularly for the OC where absolute radiances are more relevant. For that reason, it is important to maintain consistent field calibration references to track any short-term changes in the system during the campaign.

2 CALIBRATION AND RESULTS

We describe primary laboratory and secondary field radiometric calibrations used for GCAS in this section. Kowalewski and Janz [9] describe complementary laboratory calibration and characterization work that has been conducted in the past, including spectral slit function and temperature dependence characterization for GCAS.

2.1 FCS field calibrations

To characterize spectrometer performance and stability during the course of a campaign, the spectrometer response is periodically monitored by exposing it to a stable light source, even when in the field.[2] The Field Calibration System (FCS) is a mobile calibration system, originally used for as a traveling standard for the Airborne Compact Atmospheric Mapper (ACAM), a predecessor to GCAS.[13]

The FCS (shown in Figure 1) consists of a 6-inch polytetrafluoroethylene (PTFE)-coated integrating sphere (internally illuminated by a single 150-watt quartz tungsten halogen bulb), power supply, and a NASA-calibrated precision shunt and voltmeter, all housed within a transportable, rugged case. After GCAS has been integrated into a flight platform, we mount the integrating sphere onto the GCAS ground-facing plate. For most NASA aircraft, the integrating sphere can be installed without removing or otherwise modifying GCAS, which simplifies the calibration process. The FCS radiometric uncertainty has been demonstrated to vary from 2% at 300 nm to 1.5% at 400 nm and above.[8]

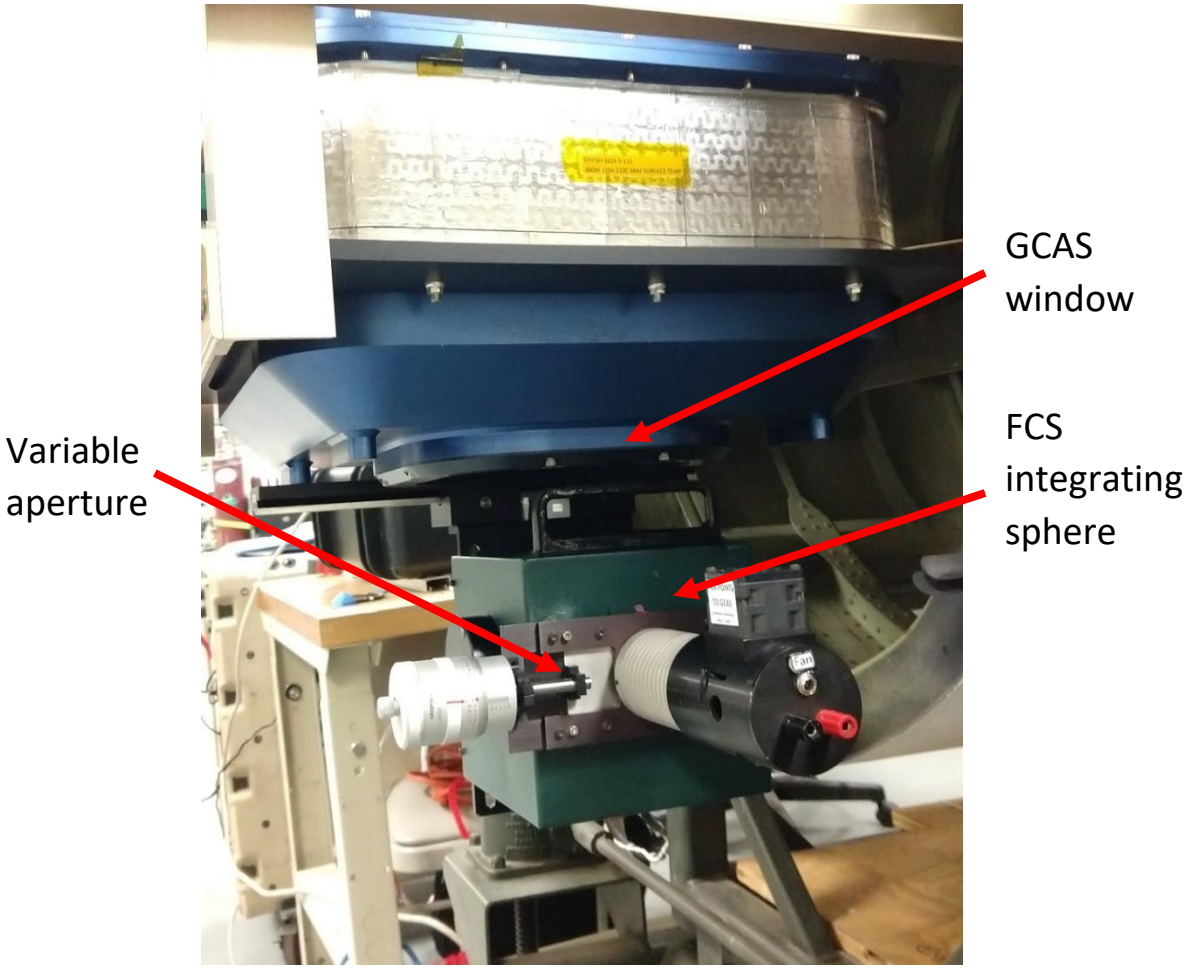

Figure 1. Image showing the FCS integrating sphere mounted to the GCAS front plate during a field calibration.

To calibrate both the AQ and OC optical paths, which are situated a few inches apart, the integrating sphere is fastened to a horizontally translating mount, so that the sphere aperture can be positioned directly below either instrument entrance aperture. A variable-width aperture on the source controls the amount of light entering the instrument. To improve the measurement precision, several image frames are collected for each spectrometer, at a predetermined sphere position, aperture setting, and integration time. These settings are maintained for subsequent calibrations to observe trends in the spectrometers over time.

An example image from an FCS calibration on 8 May 2018 (prior to the first LISTOS science sortie) is shown in Figure 2. To generate corrected count rates, we first remove the detector charge-coupled device (CCD) bias, then subtract the dark current measured when the source is turned off, and finally divide by the integration time to obtain counts per second. The images in Figure 2 are an average of over 60 frames recorded during the calibration for AQ (left) and OC (right). With the aperture of the sphere positioned about 6 inches from the GCAS window, the centermost 100 of 512 horizontally binned pixels for the AQ spectrometer and 200 of 1004 pixels for the OC spectrometer are illuminated. The width of the illuminated swath may be increased (decreased) by mounting the sphere closer (further) from the window.

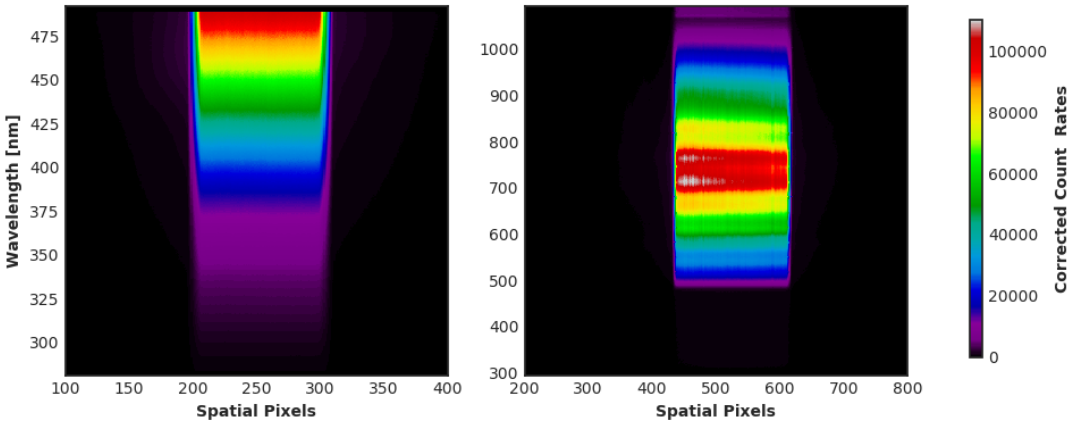

Figure 2. Example images of corrected count rates for the AQ (left) and OC (right) spectrometer FCS calibrations. Rows (columns) represent spatial (spectral) slices across the arrays.

A successful calibration monitoring system requires knowledge of the stability of the illumination system for both short-term and long-term time scales. To ensure that the lamp output is consistent between uses, the applied current is monitored using a precision, calibrated shunt wired in series with the lamp. Using a digital multimeter to measure the voltage across the shunt, we can calculate and adjust the applied current to an accuracy with a combined standard uncertainty of 0.51 milliamps.[10] Additionally, for long-term monitoring, the FCS is periodically calibrated using laboratory sources (described in the following section).

Figure 3 below demonstrates the spectral stability of the GCAS AQ and OC spectrometer response as a percentage difference from the first FCS calibration of the 2018 campaign on May 8th. For this analysis, spectral slices are averaged across the central 20 columns for both spectrometers. For AQ (upper right plot), there are spectrally dependent changes at short (<325 nm) wavelengths for a few of the tests. However, FCS output is relatively small in this region, and the comparisons have higher uncertainties here due to dark current corrections and/or stray light contamination. The same is true for wavelengths over 800 nm in the OC (upper left plot). Also for the OC spectrometer, the periodic oscillatory nature of the differences point to variations in spectrometer behavior over time, since the FCS output is generally smooth across the spectrum; changes in its output would not explain such regular fluctuations across the spectrum. For the OC calibration from 30 Nov 2018 (pink line), the 3.5% decrease in count rates at 650nm is outside the range of uncertainty we assume for FCS stability, suggesting that the OC performance has degraded somewhat during this time frame. This FCS field calibration actually occurred after the completion of the campaign, when GCAS was back in the laboratory (see Figure 6), but it is included here for completeness.

We also show a trend in count rate percentage differences for selected wavelengths near the spatial center of each spectrometer's CCD array: 400 nm for the AQ (Figure 3, lower plot, in black) and 700 nm for the OC (in red). There is a small downward trend in the data, with correlation coefficients of around -0.77 for each spectrometer's linear fit. If we assume FCS output is constant over time, the results point to strong confidence in the downward trend, around 2 – 3% for the spectrometers during the course of the field calibrations and demonstrates the level of precision that can be obtained with the FCS during a field campaign. However, for the LISTOS field campaign we are only concerned with data between 3 July 2018 and 6 September 2018, during which time the linear downward drift is around 0.7% for AQ

and 1.0% for OC. For typical trace gas retrieval applications, this short-term decrease in sensitivity can be ignored. The error bars in this trend plot represent the combined uncertainty of the FCS stability [8] and the signal noise in the FCS spectral slices for each date.

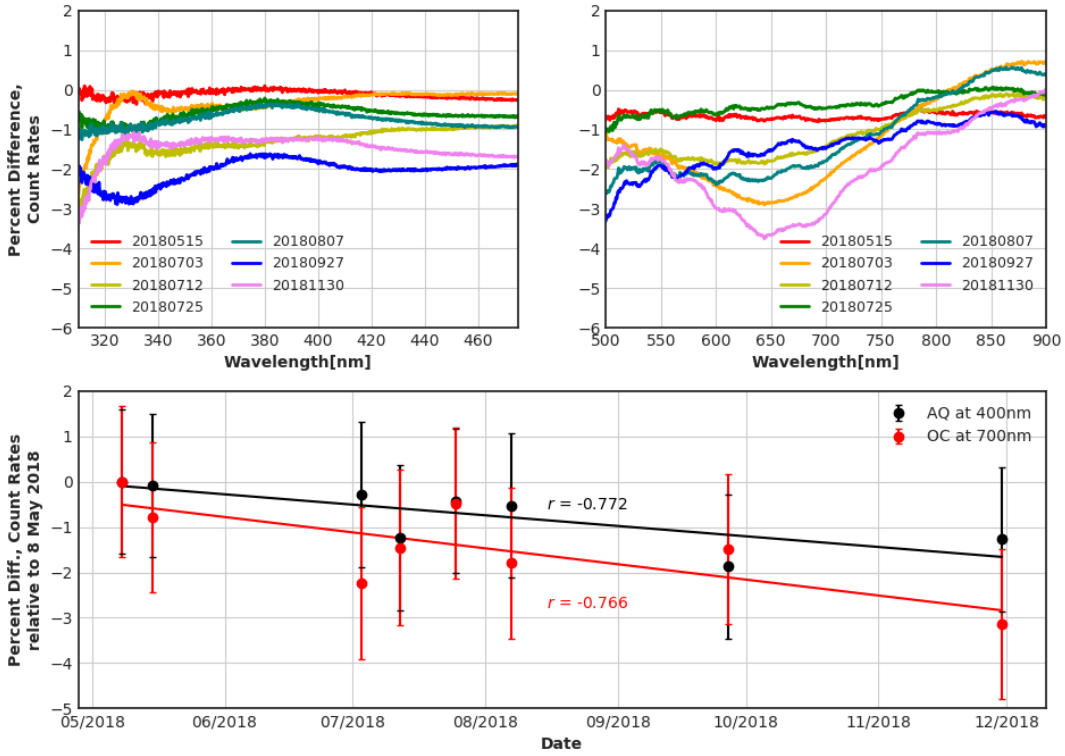

Figure 3. *Upper plots*: AQ and OC spectral count rate percentage differences, compared to the FCS calibration on May 8th. *Lower plot*: trend in the differences, relative to May 8th, for selected wavelengths at the center of the array.

Figure 4 demonstrates the spatial stability of the GCAS responsivity, shown as the percentage difference from the initial FCS calibration on 8 May 2018. For each test date, spatial slices are averaged across the central rows (210 – 295 for AQ and 450 – 600 for OC). The spatial averages were then normalized to the value at the center of the illuminated swath (pixel 252 for AQ and pixel 525 for OC) to demonstrate the spectrometer responsivity on either end of the illuminated field-of-view. For the AQ (upper left plot), the responsivity shows little variation across spatial pixels, differing by no more than 2% anywhere in the array. For the OC (upper right plot), there is a positive bias for pixels to the left-of-center (up to 7%) versus the right-of-center (up to -5%). We also calculated responsivities for spatial rows in the upper and lower portions of the CCD arrays, but saw no significant difference from the results at the central portions of the CCDs.

The lower plot describes a trend in spatial responsivity over time. Here the spatial count rates within the slice are averaged, then divided by the maximum in the same range, similar to a technique described by Gatebe.[5] Any deviation from unity describes a non-uniform spatial distribution across the CCD array. For the AQ (Figure 4, lower plot, in black), the value is between 1.00 and 1.01 for all test dates, whereas for the OC (in red) it is between 0.94 and 0.95, reflecting the left-to-right bias described above. We observe that responsivity is overall higher (less uniform) for the OC compared to AQ, but that responsivity for each spectrometer does not drift more than 1% over the course of the campaign and therefore would not require any post-campaign calibration adjustments. This is especially important for the OC spectrometer, where the signal varies dramatically across the array. Since GCAS will have an absolute calibration in the laboratory both before and after field deployments (described below), spatial variations are acceptable so long as they remain stable during the course of a campaign. The error bars in this trend plot represent the standard

deviation of the normalized spatial slices (the signal noise) from the FCS for each date. Specific values for AQ/OC responsivity are provided in Table 1, along with their percentage differences from the initial test, for reference.

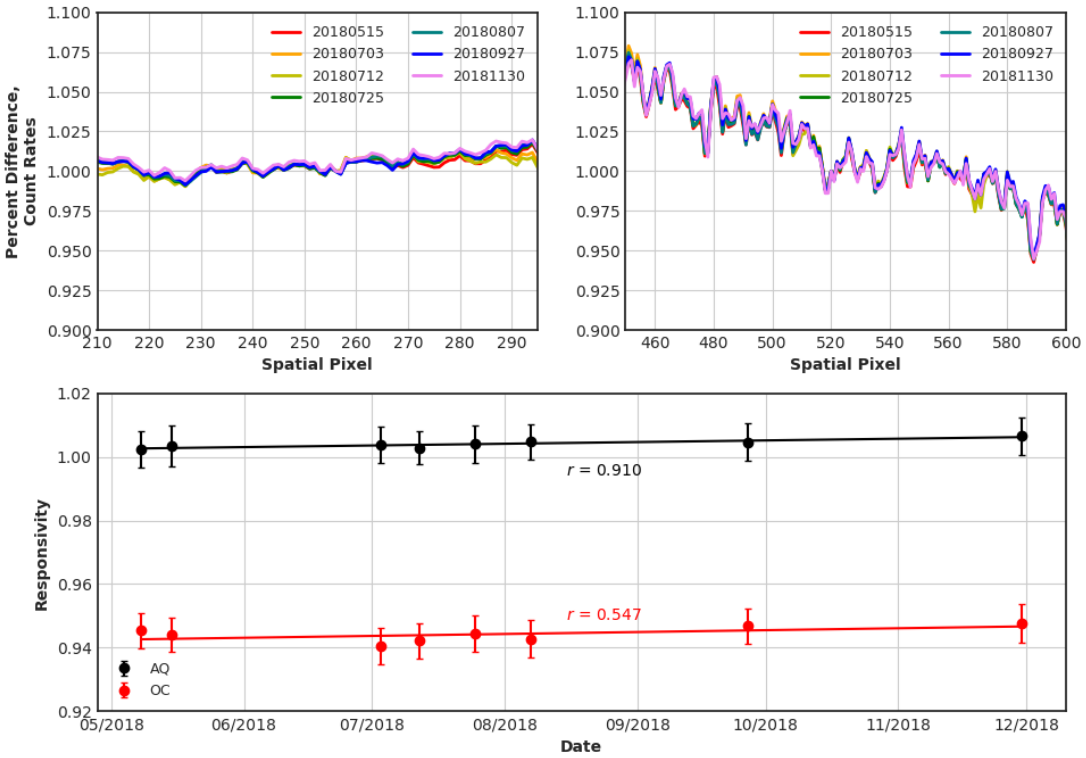

Figure 4. *Upper plots*: AQ and OC responsivity percentage differences, compared to the FCS calibration on May 8th. *Lower plot*: trend in the responsivity, relative to May 8th, over time.

Table 1. AQ and OC responsivities in columns 1 and 3. AQ and OC responsivity percentage differences from the value at 8 May 2018 in columns 2 and 4.

DATE	AQ SENSITIVITY	PERCENT DIFFERENCE FROM MAY 8	OC SENSITVITY	PERCENT DIFFERENCE FROM MAY 8
MAY 8	1.003	-	0.945	-
MAY 15	1.004	0.10	0.944	-0.14
JUL 3	1.004	0.12	0.940	-0.52
JUL 12	1.003	0.04	0.942	-0.35
JUL 25	1.004	0.16	0.944	-0.11
AUG 7	1.005	0.22	0.943	-0.28
SEPT 27	1.005	0.21	0.947	0.15
NOV 30	1.007	0.41	0.948	0.25

2.2 Laboratory radiance transfers

The FCS calibrations are used to provide information on the in-field stability of the spectrometers so that the primary laboratory measured instrument sensitivity can be adjusted if necessary. Before and after each field deployment, we characterize the radiance of the FCS first by transferring a NIST-calibrated quartz-tungsten-halogen (traditionally denoted as FEL) lamp irradiance to an independent MS257 double monochromator (Newport Corporation) equipped with an input diffuser, using a procedure previously described by Kowalewski and Janz.[10] In this process, Equation 1 is used to derive the radiance of the FCS from 250 nm – 900 nm:

$$L_{\lambda,sphere} = \frac{C_{\lambda,sphere}}{C_{\lambda,FEL}} * L_{\lambda,FEL} * \frac{D^2_{sphere}}{D^2_{FEL}} * G: \quad (1)$$

where $C_{\lambda,FEL}$ are the count rates measured by the MS257 viewing the FEL, $C_{\lambda,sphere}$ are the count rates measured by the MS257 viewing the sphere, $L_{\lambda,FEL}$ is the radiance of the FEL-illuminated input diffuser, D_{FEL} and D_{sphere} are the distances of the FEL and the sphere to the MS257, respectively, and G is a scaling factor related to the effective apertures of the sphere and input diffuser. We use several FEL lamps and two different sphere-to-diffuser distances to generate, and later average, the measured spectral radiances for the FCS. By monitoring the FCS radiance before and after a campaign, we can assess how changes in FCS behavior contributed to any intra-campaign trends observed from the field calibrations.

We utilize the same radiance transfer procedure for a larger 20" PTFE-coated integrating sphere (named "Junior"). Junior houses four 150-watt quartz tungsten halogen lamps whose stability has been shown to be better than 1% from 400 nm – 1000 nm over time.[4] Junior is then used to derive spectrally-dependent calibration sensitivities for GCAS in the laboratory since Junior can illuminate more spatial rows, provide a higher output radiance, and is more stable compared to the FCS. The GCAS calibration sensitivity is defined using Equation 2 as:

$$GCAS_{\lambda,cal} = \frac{GCAS_{\lambda,sphere}}{L_{\lambda,sphere}} \quad (2)$$

where $GCAS_{\lambda,sphere}$ are the bias-dark-integration time corrected count rates from GCAS viewing Junior and $L_{\lambda,sphere}$ is the radiance transferred from the FEL lamps and Equation 1. The ratio of the sensitivities over time represents the true instrument spectral sensitivity change. By monitoring the GCAS calibration sensitivity before and after a campaign, we can assess how changes in spectrometer behavior contributed to any intra-campaign trends observed from the field calibrations.

Figure 5 demonstrates the pre- (26 Jan 2018) and post- (17 Apr 2019) campaign laboratory calibration comparisons for FCS radiances (in green). For wavelengths longer than 500 nm, FCS output decreased by about 2.5% during the 15 months between calibrations (about 0.15% per month, assuming a linear drift). The direction of the shift is consistent with the trends we observed in the FCS field calibration trends for OC, which were earlier attributed to a decrease in spectrometer performance due to the oscillatory shape of the spectral differences. There is also an increase in FCS radiance at wavelengths smaller than 450 nm. This change may be an artifact of the radiance transfer procedure, or it may be real and reflect a degradation of the diffuser surface of the FCS in the shorter wavelengths. However, based on the field calibration downward trends with strong linear correlation coefficients, we assume that the FCS field calibration would have captured such an increase in FCS output, and that any change in the FCS system occurred before (after) the first (final) field test, perhaps as a result of shipping or extended storage. Alternatively, a combination of FCS changes and spectrometer sensitivity changes, described next, is more likely.

GCAS calibration sensitivities (Figure 5, in black) show an overall increase of 2 – 3% during the pre- (21 Dec 2017) to post- (11 December 2018) comparison, which would correspond to an increase of around 1% during the course of the LISTOS campaign, assuming a linear drift. Again, it is difficult to determine at what point in time this change would have occurred. It is unlikely that spectrometer sensitivity would have decreased (as is suggested from the downward trend in FCS field calibrations) and then increased (as is possible from the increase in calibration sensitivity) over the course of year. It is more likely that these sensitivity changes occurred outside our period of field measurements, and therefore were not captured during the FCS field calibrations. The error bars in this plot represent the combined uncertainty in the radiance transfer procedure described above.

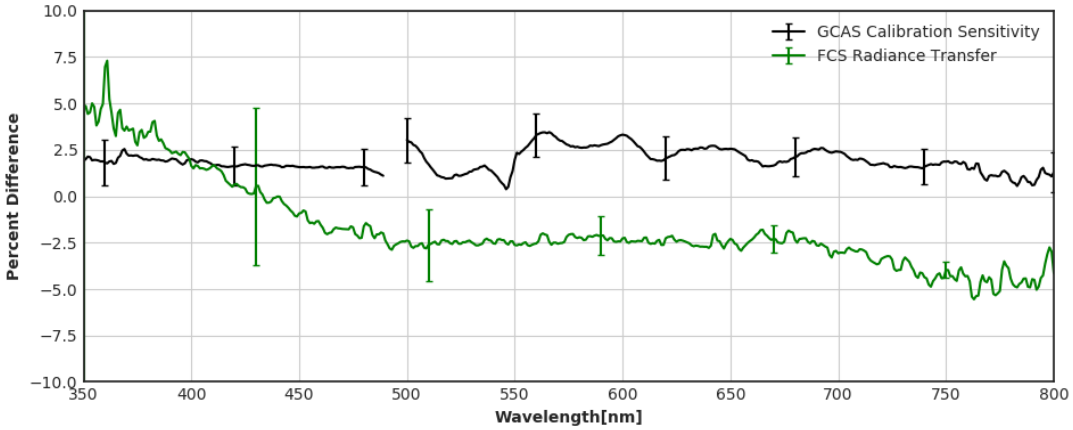

Figure 5. Percentage differences in post-campaign GCAS calibration sensitivities (black) and ACS transferred radiances (green), relative to the pre-campaign calibrations.

These results point out the need for more frequent laboratory radiance transfers, so that we can better pinpoint times when system changes occur and whether they should be accounted for during post-processing. Figure 6 visually demonstrates the gaps in time between FCS field calibrations (in blue), laboratory FCS radiance calibrations (in green), and laboratory GCAS radiance calibrations (in black). In particular, the pre-mission GCAS calibration and the post-mission FCS radiance calibration occurred several months prior to and after the series of field calibrations, respectively, during which time storage or shipping may have contributed to system changes. However, so long as neither the FCS nor the GCAS radiance calibration trends differ by more than a percent or so during the course of a campaign (which are generally on the order of a few months, like LISTOS, shaded in light blue), no further post-processing of data is necessary, at least for trace gas retrievals which are only dependent on relative radiances.

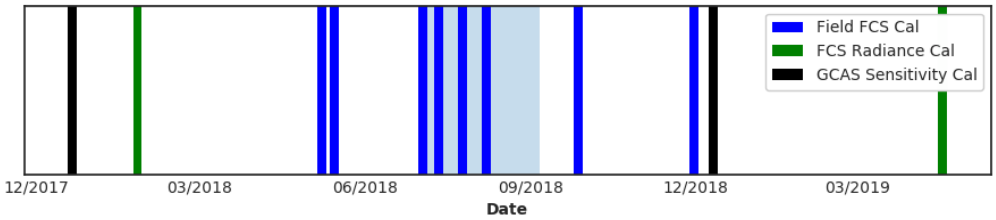

Figure 6. Calibrations conducted by date for the period before, during, and after LISTOS. The LISTOS campaign period (3 July – 6 September 2018) is shaded in light blue.

3 SUMMARY

We have demonstrated an in-field calibration routine used to check the spectral and spatial stability and performance of GCAS spectrometers while on field deployments. Results showed that during the course of the field measurements, spectral responsivity decreased by about 1%, attributable to some combination of FCS and GCAS system changes. These results are well within error budgets for typical trace-gas retrieval algorithms and indicate that no post-processing of calibration coefficients is warranted for this campaign. However, radiance transfer calibrations of the FCS conducted before and after the campaign demonstrate measureable differences in FCS that appear to occur outside the field campaign timeframe. These results indicate that to reduce the risk for future campaigns, more frequent laboratory radiance transfer calibrations of the FCS should be implemented to properly separate any long-term drift or anomalous behavior of the FCS from short-term in-field stability.

ACKNOWLEDGEMENTS

Peter Pantina is supported under NASA contract NNG17HP01C.

REFERENCES

[1] Bell, M. L., et al., “Ozone and short-term mortality in 95 US urban communities, 1987 – 2000,” Journal of the Amer. Medical Association 292, 2372 – 2378 (2004).
[2] Bohn, B. and Lohse, I., “Calibration and evaluation of CCD spectrometers for ground-based and airborne measurements of spectral actinic flux densities,” Atmos. Meas. Tech. 10, 3151 – 3174 (2017).
[3] Buchwitz, M., et al., “Atmospheric carbon gases retrieved from SCIAMACHY by WFM-DOAS: version 0.5 CO and CH4 and impact of calibration improvements on CO2 retrieval,” Atmospheric Chemistry and Physics European Geosciences Union 6, 2727-2751 (2006).
[4] Butler, J. J., “Calibration of a radiance standard for the NPP/OMPS instrument,” Proc. SPIE 7106, Sensors, Systems, and Next-Generation Satellites XII, 71060Z (2008).
[5] Gatebe, C. K. et al., “Characterization of errors in the use of integrating-sphere systems in the calibration of scanning radiometers,” Applied Optics 46, 7640 – 7651 (2007).
[6] Jhun, I. et al., “The impact of nitrogen oxides concentration decreases on ozone trends in the USA,” Air Quality Atmosphere and Health 8, 283 – 292 (2015).
[7] Judd, L. et. al., “Lessons Learned from High Spatiotemporal Airborne NO2 Measurements in Urban Coastal Regions,” Amer. Geophysical Union Fall Meeting, abstract #A53C-02, (2018).
[8] Kowalewski, M. G., and Janz, S. J., “Remote sensing capabilities of the Airborne Compact Atmospheric Mapper,” Proc. SPIE 7452, 74520Q (2009).
[9] Kowalewski, M. G, and Janz, S. J., "Remote sensing capabilities of the GEO-CAPE airborne simulator," Proc. SPIE 9218, 92181I (2014).
[10] Kowalewski, M. G., and Janz, S. J, “Comparison of spectral radiance responsivity calibration techniques used for backscatter ultraviolet instruments,” Metrologia 52, 145 – 154 (2015).
[11] Kuester, M. A., et al., “Radiometric calibration concept of imaging spectrometers for a long-term ecological remote sensing project,” (2010).
[12] Levelt, P. F., et al., "The ozone monitoring instrument," IEEE Transactions on Geoscience and Remote Sensing 44, 1093-1101 (2006).
[13] Liu, C., et al., “Characterization and verification of ACAM slit functions for the trace-gas retrievals during the 2011 DISCOVER-AQ flight campaign,” Atmos. Meas. Tech. 8, 751 – 759 (2015).
[14] Miller, P. J., “Long Island Sound Tropospheric Ozone Study (LISTOS),” Amer. Geophysical Union Fall Meeting (2018).

[15] Nowlan, C. R., et al., “Nitrogen dioxide and formaldehyde measurements from the GEOstationary Coastal and Air Pollution Events (GEO-CAPE) Airborne Simulator over Houston, Texas,” Atmos. Meas. Tech. 11, 5941 – 5964 (2018).
[16] Richter, A., et al., “Increase in tropospheric nitrogen dioxide over China observed from space,” Nature 437, 129 – 132 (2005).
[17] Qu, J. J, et al., “Integrating the cross-sensor calibration and validation system for GEOSS support," Proc. SPIE 7151, 715109 (2008).
[18] Werdell, P. J., “The Plankton, Aerosol, Cloud, ocean Ecosystem (PACE) mission: Status, science, advances,” Bulletin of the American Meteorological Society, (2019).
[19] Woodward, J. T., et al., "Hyperspectral imager characterization and calibration," 2009 IEEE International Geoscience and Remote Sensing Symposium, II77-II80 (2009).
[20] Zhang, M., et al., “Atmospheric correction of hyperspectral airborne GCAS measurements over the Louisiana Shelf using a cloud shadow approach,” International Journal of Remote Sensing 38, 1162 – 1179 (2016).